EARTH SURFACE PROCESSES AND LANDFORMS
Earth Surf. Process. Landforms **36**, 1705–1714 (2011)

Published online 27 June 2011 in Wiley Online Library
(wileyonlinelibrary.com) DOI: 10.1002/esp.2179

Numerical modelling of combined erosion and weathering of slopes in weak rock

M. Huisman,[1]* J. D. Nieuwenhuis[2] and H. R. G. K. Hack[3]
[1] Bluewater Energy Services BV, Mooring & Subsea Technology, Hoofddorp, Netherlands
[2] Delft University of Technology, Civil Engineering & Geosciences, Delft, Netherlands
[3] University of Twente, Faculty ITC, Enschede, Netherlands

Received 22 March 2010; Revised 2 May 2011; Accepted 8 May 2011

*Correspondence to: M. Huisman, Bluewater Energy Services BV, Mooring & Subsea Technology, Hoofddorp, Netherlands. E-mail: marco.huisman@bluewater.com

ESPL
Earth Surface Processes and Landforms

ABSTRACT: Due to various decay processes associated with weathering, the stability of artificial slopes in weak rocks may be affected well within their envisaged engineering lifetime. Conceptually, the decay following the initial stress release after excavation can be described as a process seeking equilibrium between weathering and erosion. The extent to which such an equilibrium is actually reached influences the outcome of the weathering-erosion decay process as well as the effects that the decay has on the geotechnical properties of the exposed rock mass, and thus ultimately the stability of slopes affected by erosion and weathering. This paper combines two conceptual models for erosion and weathering, and derives a numerical model which predicts the resulting slope development. This can help to predict the development of a slope profile excavated in a weak rock in time, and can be extended with the addition of strength parameters to the weathering profile to enable prediction of slope stability as a function of time. Copyright © 2011 John Wiley & Sons, Ltd.

KEYWORDS: erosion; weathering; denudation; numerical modelling; slope stability; shale

Introduction

The problem of infrastructure works that become unsafe with time due to decay of rock and soil masses in artificial and natural slopes is a well-known feature in every part of the world. Many economically hazardous and potentially life-threatening mass movements in artificial as well as natural slopes are caused or facilitated by decay of soil and rock (Hencher and McNicholl, 1995). This time-related decay of soil and rock affects all engineering structures that involve natural, *in situ* materials, and is easily recognized in artificial, engineered slopes in rapidly weathering and easily eroding shales.

The combined processes of weathering and erosion will cause decay of any rock mass exposed in a slope, with stress release and stress–strain redistribution as catalysts; an elaborate example of this is given by Nieuwenhuis (1991) for relatively weak ground masses that show rapid deterioration. The relative rates of erosion and weathering determine how the rock mass actually develops and as will be shown later, the ratio of those rates can change within a single slope as a function of both space (i.e. at different locations in the slope) and time. Depending on the relative rates, three main decay situations can be distinguished:

- imbalance favouring erosion;
- equilibrium between weathering and erosion;
- imbalance favouring weathering.

Assuming that natural hillslopes are in equilibrium, excavations are by definition a disturbance of that equilibrium, and the development of the excavation profile is an evolutionary model. The boundary conditions for this model are set by the principal slope properties after excavation: the slope profile and the remaining weathering profile resulting from weathering of the original surface, prior to excavation. The response of the slope material to the environmental conditions then determines the slope evolution after excavation, and this paper combines conceptual models for erosion and weathering of slopes in order to assess what stages of equilibrium and imbalance an artificial slope can go through in its engineering lifetime.

Carson (1969) provides an overview of what can be considered the starting point of mathematical modelling of such processes, through process-response models. The development of such models was done in three separate steps: the identification of a particular process (or set of processes) and the variables which control the rate at which the processes operate; the definition of the way in which that process operates to change the form of the system in an infinitely small increment of time; and the extrapolation of the geometric change in that small increment of time until the system reaches equilibrium.

This process-based approach saw pioneering work done by Kirkby and by Ahnert. Kirkby (1971) focused on a mass balance approach and the resulting continuity equation in differential form. Ahnert's approach (Ahnert, 1976) investigated the equilibrium (or lack thereof) of debris supply and transport, which is again essentially a mass balance, but without the differential equations of Kirkby. He found that the assumed transport mechanism has a major influence on the resulting slope profile,

with the two possibilities for a control volume (i.e. the slope) being complete removal of eroded material, or point-to-point transport with re-deposition, resulting in an accumulation of re-deposited erosion products at the toe of the slope.

As is apparent when setting up process-based slope development models, a great number of parameters needs to be considered, and the number and non-linearity of their parameters renders their predictions ambiguous and often unrealistic (Brazier *et al.*, 2000). A revival of conceptual models, such as the one described in this paper, may be helpful to obtain somewhat crude but nevertheless reliable predictions and also show how processes may interact on a fundamental mathematical level, the second step defined by Carson (1969) as being essential for process-based modelling. It is for these two reasons, to find and understand physical relations and to compare the outcome with available field data, that a conceptual model is derived in this paper.

Models for Weathering and Erosion

The combined action of weathering and erosion can be quantified by combining two concepts supported in the literature on this subject into a conceptual model. This model combines the Bakker – Le Heux erosion model (Bakker and Le Heux, 1946, 1952) with a weathering penetration model in which the penetration rate is a decreasing function of the thickness of the weathering cover (Heimsath *et al.*, 1997).

With regard to erosion, Bakker and Le Heux (1946, 1952) formulated two models for slope evolution with time, in order to explain slope forms found in nature, in particular those in high mountain areas in Anatolia (Turkey) where the slopes are covered at their toe by pediments. In both models the down-wasted weathering products are deposited in the form of a growing scree slope at the original slope's toe. The nature of the down-wasting process (rolling downward, landslides, avalanches or water/snow erosion) was not discussed. For the down-wasting of the exposed slopes two potential mechanisms were considered: parallel slope retreat through down-wasting of slices of constant thickness over the full slope height (Bakker and Le Heux, 1946), and rotating slope retreat through down-wasting of triangular slices that are thick at the top and thin at the toe (Bakker and Le Heux, 1952). The second mechanism results in a decreasing slope angle. It must be noted that both models are applicable to slopes where the eroding particles are small compared with the slope size.

Whereas Bakker and Le Heux (1946) found that the parallel slope retreat mechanism appeared well applicable to the Anatolian mountains, the rotating slope retreat mechanism seems to be a better fit for Western European slopes. In the investigated slopes of road cuts in the research area near Tarragona in Spain, angular rotation of the retreating slope face has been observed. In view of this the rotating slope retreat model has been adopted here, and developed further. This model has been described in detail by Hutchinson (1998), who performed small-scale field tests that showed good agreement between the predicted and measured final slope profiles.

One of the few examples of a quantified relation for weathering depth and time is given by Heimsath *et al.* (1997), who determined soil production rates (calculated from *in situ* produced cosmogenic ^{10}Be and ^{26}Al in bedrock samples) as a function of the thickness of the weathered soil cover for hillslopes in northern California. The soil production rate, which is equal to the increase of the thickness of the weathered zone in time, is shown to decrease with an increasing thickness of that same weathered zone. A similar formulation was used to integrate weathering into slope erosion models by Martin (2000). This is the likely development for a weathering profile as found in the case study slope described later in this paper, in which the material underneath the weathered cover is protected from the dominant weathering processes.

Since the thickness of the weathered zone in slopes is affected by the erosion acting on it, applying this same weathering model to slopes that evolve in a rotating manner as described by Bakker and Le Heux (1952) leads to a set of equations that describe the development of the slope profile as well as the penetration of the weathering front. This set of equations can be solved numerically by time-stepping. Depending on erosion and weathering penetration rates, different decay situations are shown to occur at a given point in time for different locations along the slope profile, just as different situations occur for a given location along the slope profile for different exposure times.

The Bakker–Le Heux model for erosion and the Heimsath model for weathering are described in more detail in the following paragraphs.

Erosion: Bakker–Le Heux

The rotating Bakker–Le Heux model describes the ultimate slope profile of a linearly retreating, initially straight slope, excluding erosion from any surface above the slope. The model makes the following assumptions, as summarized by Hutchinson (1998):

- An initially straight slope of uniform material of inclination β exists, steep enough for debris removal not to be transport-limited.
- The slope has horizontal ground at its toe and past its crest.
- No standing water is present at the foot.
- In a given amount of time, weathering weakens the surface material, giving rise to retreat of all parts of the exposed free face due to the erosion of fine debris. This can be approximated theoretically by infinitesimal increments; larger falls, where volumes larger than the individual particles are affected, are not considered.
- The resulting debris accumulates at the cliff foot as a rectilinear scree with a constant slope angle α ($\alpha < \beta$).
- Beneath the accumulating scree, the rock surface is protected from further erosion, while the rock face above continues to retreat.
- Thus, with time, a convex-outward shape is produced in the surface of the intact rock beneath the scree. Ultimately the original cliff develops into a straight slope with an inclination equal to the scree angle α, to which, in its last formed upper part, the underlying convex rock core is tangential.

Basically, the model considers a decreasing angle of the apex line through the origin (the initial slope toe) and the upper section of the slope. A change in this angle results in a small increment of the eroded volume, and thus a corresponding small increment in the debris covering the toe of the slope in a scree wedge, while taking into account volume changes and erosion at the toe (Figure 1).

The original Bakker–Le Heux model describes only the ultimate state of the eroded slope and gives an expression for the ultimate rock profile, as used by Hutchinson (1998) for a small-scale field check. The ultimate profile of the convex rock core underneath the scree is given by the following expression (for $c \neq \frac{1}{2}$):

$$y = az - (a-b)z\left[\frac{h^2 + (1-2c)z^2}{h^2}\right]^{\frac{c-1}{1-2c}} \quad (1)$$

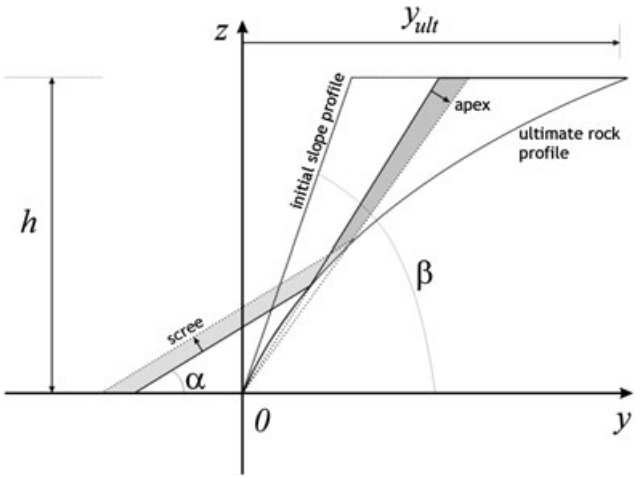

Figure 1. Definition sketch of the Bakker–Le Heux model for slope retreat (after Hutchinson, 1998).

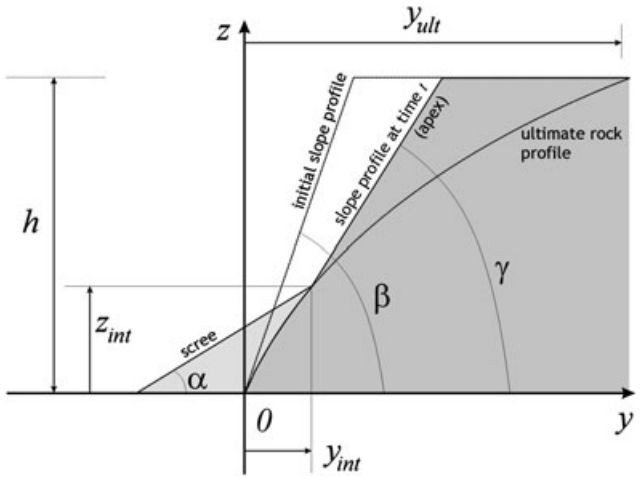

Figure 2. Definition of parameters in time-dependent model for slope retreat.

with parameters y and z as defined in Figure 1 ($y=0$ and $z=0$ at the foot of the initial slope profile), and:

a	cotangent of stable slope angle for scree, cot(α)	[−]
b	cotangent of initial slope angle at time of excavation, cot(β)	[−]
c	1 – (volume of rock) / (volume of scree)	[−]
h	height of the slope	[m]

A ratio of the volumes of rock to scree smaller than 1 (i.e. $c>0$) indicates a volume increase of material during erosion and sedimentation. A value larger than 1 ($c<0$) indicates removal of sediment at the foot of the slope. The model is not defined for $c=0.5$, and $c=1$ is the maximum value. For the results presented in this paper, it has been assumed that c is constant in time but this assumption does not affect the methodology. This parameter is not only the result of the rock mass and debris properties, but also of outside influences – e.g. human action (physical removal of debris at the toe of the slope), further erosion in the debris zone, etc. If there is no removal of debris from the site, c can be predicted by considering the unit weights of the *in situ* material and the debris. For artificial slopes such as road cuts, outside influences are likely to act on the debris and thus affect c, which implies that this parameter will vary from site to site.

The development of the slope profile in time can be simulated quantitatively by assigning a time function to the inclination of the apex line through the origin γ and taking appropriately small time steps. At any time t, the profile of the eroded rock surface is then given by (Figure 2):

$$\text{if } 0 \le z \le z_{int} \Rightarrow y_e = az - (a-b)z\left[\frac{h^2 + (1-2c)z^2}{h^2}\right]^{\frac{c-1}{1-2c}} \qquad (2)$$
$$\text{if } z_{int} \le z \le h \Rightarrow y_e = \frac{z}{\tan(\gamma)}$$

with

y_e	y-coordinate of eroded rock profile	[m]
z	vertical coordinate	[m]
z_{int}	z-coordinate of interception between scree wedge and eroded rock	[m]
γ	inclination of the apex line through the crest and toe (function of time)	[°]

The profile of the overlying scree is given at any time t by:

$$\text{if } 0 \le z \le z_{int} \Rightarrow y_s = y_{int} - \frac{z_{int} - z}{\tan(\alpha)} \qquad (3)$$

with

y_s	y-coordinate of scree profile	[m]
y_{int}	y-coordinate of interception between scree wedge and eroded rock	[m]

Field data gathered in the course of this study suggest that the slope retreat is linear in time at least for the first years after excavation, as will be discussed later in this paper.

If this observed linear trend for γ is extrapolated until the stable scree angle α is reached, then:

$$\begin{aligned} &\text{if } 0 \le t \le \frac{\beta-\alpha}{R_s} \quad \Rightarrow \quad \gamma = \beta - R_s t \\ &\text{if } t \ge \frac{\beta-\alpha}{R_s} \quad \Rightarrow \quad \gamma = \alpha \end{aligned} \qquad (4)$$

with

R_s	rate of angular slope retreat	[°/year]
t	time	[years]
α	stable slope angle for scree	[°]
β	initial slope angle at time of excavation	[°]

It should be noted that non-linear functions of $\gamma(t)$ would also be allowed. The data reported by Hutchinson (1998) suggest that the rate of slope retreat decreases with longer exposure times. However, the time span covered by the field studies undertaken for the present paper is too short to confirm this. The observed linear decrease may not remain valid for longer time intervals. Furthermore it is likely that the trend will be influenced by the weathering of the slope surface, and Equation (4) should be considered as an example only. However, the methodology for derivation of the model and the qualitative results do not depend on the nature of Equation (4).

Continuity of the rock profile in y_{int} and z_{int} (the coordinates of the point where the surface of the scree wedge intercepts the intact rock, Figure 2) gives:

$$y_{int} = \frac{z_{int}}{\tan(\gamma)} \tag{5}$$

$$z_{int} = \frac{h}{1-2c}\sqrt{(1-2c)\left(e^{\frac{1-2c}{c-1}\ln\left(\frac{a\tan(\gamma)-1}{(a-b)\tan(\gamma)}\right)}-1\right)} \tag{6}$$

with

a	cotangent of stable slope angle for scree, cot(α)	[–]
b	cotangent of initial slope angle at time of excavation, cot(β)	[–]
h	slope height	[m]

Starting at the point defined by the coordinates given by Equations (5) and (6), the scree wedge stretches downward with an inclination equal to α and the rock face upward with an inclination γ (Figure 2).

At any time t, the profiles of the eroded rock surface and of the overlying scree are given by Equations (2) and (3), in which y_{int} and z_{int} are found by combining Equations (5) and (6) with (4). Provided that an expression for $\gamma(t)$ is known, Equations (2) and (3) therefore define the slope profile and the profile of the eroded rock core at any time t. The limiting case of this slope development model is a convex, uneroded core of rock with a curve that has an inclination equal to the scree angle α at $\gamma(z=h)$ and equal to the initial slope angle β in the origin. The curved rock core is covered completely by scree inclined at angle α in this limiting case.

Weathering Penetration: Heimsath

The empirical relation derived by Heimsath *et al.* (1997) has the following general shape defining the weathering depth as a function of time, with the penetration rate of the weathering front inversely proportional to the thickness of the weathered cover:

$$\frac{dD_w}{dt} = e^{A+BD_w} \tag{7}$$

with

D_w	depth (thickness) of weathered layer	[m]
A, B	constants	

A relation of this form has also been adopted by Martin (2000) to combine weathering and erosion. It must be noted that it only defines the thickness of the weathered cover in time, not the intensity of weathering in that cover, and this is an important aspect: if the goal is to calculate the amount of sediment available for transport, as is the basis of models such as that of Anderson and Humphrey (1989) and Tucker and Slingerland (1994), this alone would not be sufficient, and this especially applies to weak rock in which even weathered material may show a considerable resistance against erosion. This is not further addressed in this paper, since the mode of erosion is pre-defined (by the Bakker–Le Heux model) and the erosion rate is empirically fitted to field observations.

Note that if in Equation (7) $A=\ln(W_s)$ and $B=-1/W_s$, with W_s a penetration rate coefficient (m/ln(year)) other than zero, this can be simplified to:

$$\frac{dD_w}{dt} = \frac{W_s}{1+t} \tag{8}$$

In that case, the weathering depth at any time t can be directly computed from:

$$D_w = W_s \ln(1+t) \tag{9}$$

Equation (9) assumes that there is zero erosion from the surface; if erosion occurs, the actual weathering depth will be less than predicted by this equation.

Following this model, the weathering penetration rate decreases with increasing thickness of the weathering mantle. Since the weathering mantle may be subject to erosion, the penetration rate of the weathering front is affected by the erosion rate. In order to investigate the interaction between erosion and weathering penetration processes acting on a slope, the erosion–time description of Equations (2) and (3) are combined here with the empirical weathering-time description of Equation (7). In this combination (to be described in the next paragraph) the term 'conceptual model' needs some explanation. The Bakker–Le Heux model is conceptual as it prescribes the nature of slope denudation as linearly increasing upslope. In the previous paragraph a linear rate of rotation was added (although the time-step computation described in this paper allows for non-linear rotation rates). Heimsath's weathering model is conceptual only in the sense that weathering is considered to be independent from z (vertical location in the slope). Heimsath's further description is empirical however, and based on field observations. As explained previously the same applies to the function that describes the slope angle as a function of time, $\gamma(t)$.

Combined Model for Erosion and Weathering Penetration

Consider a time interval Δt starting at time t, with a weathered zone having thickness $D_w|_t$ (Figure 3). During the interval Δt, some erosion will occur above the point of intercept of the scree cover and the rock core. The slope profile will be changing as described by the following equations:

$$\begin{cases} \text{if } z > z_{int} \begin{cases} y_e|_t = \dfrac{z}{\tan(\delta|_t)} \\ y_e|_{t+\Delta t} = \dfrac{z}{\tan(\delta|_{t+\Delta t})} \\ \Delta y_e = y_e|_{t+\Delta t} - y_e|_t = \dfrac{z}{\tan(\delta|_{t+\Delta t})} - \dfrac{z}{\tan(\delta|_t)} \end{cases} \\ \text{if } z \le z_{int} \begin{cases} y_e|_{t+\Delta t} = y_e|_t \\ \Delta y_e = y_e|_{t+\Delta t} - y_e|_t = 0 \end{cases} \end{cases} \tag{10}$$

The angle δ is the inclination of the intact rock profile (i.e. the slope without the scree cover), and depends on the vertical location, z. In the upper slope, above the scree and thus for $z > z_{int}$, δ is equal to γ as defined in Equation (4). Below the scree top, for $z < z_{int}$, δ is equal to the angle of the tangent to the rock core. The angle δ is given by:

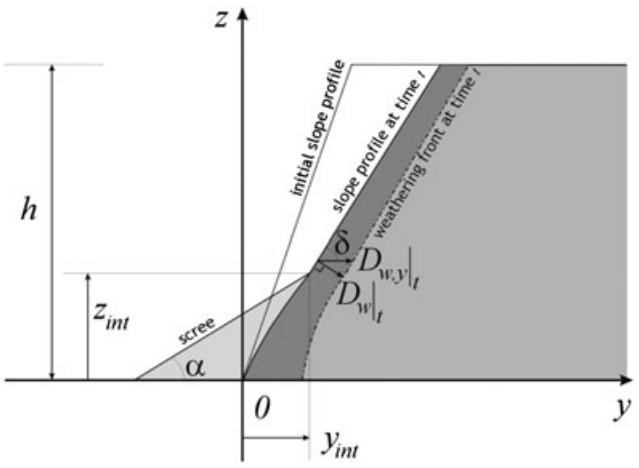

Figure 3. Representation of a weathering profile developed in a slope at time *t*.

exact equilibrium, and the third a case where erosion exceeds penetration of weathering. Since the weathering depth cannot become negative, the weathering depth in the latter case is restricted to values larger than or equal to zero.

In terms of *y*-coordinates, the weathering front is defined by:

$$y_w|_{t+\Delta t} = y_e|_{t+\Delta t} + D_{w,y}|_{t+\Delta t} \tag{13}$$

with

y_w	horizontal coordinate of weathering penetration front	(m)

Using Equation (13) the profile of the weathering front can be calculated through an iterative procedure with the boundary condition:

$$D_w|_{t=0} = 0 \Rightarrow y_w|_{t=0} = y_e|_{t=0} \tag{14}$$

$$\begin{aligned} &\text{if } 0 \le z \le z_{int} \quad \Rightarrow \quad \delta|_t = \operatorname{atan}\left(\frac{S}{aS + ah^2\left(\frac{-S}{h^2}\right)^{\frac{1-c}{2c-1}} - ay^2\left(\frac{-S}{h^2}\right)^{\frac{1-c}{2c-1}} - bh^2\left(\frac{-S}{h^2}\right)^{\frac{1-c}{2c-1}} + by^2\left(\frac{-S}{h^2}\right)^{\frac{1-c}{2c-1}}}\right) \\ &\text{if } z_{int} \le z \le h \quad \Rightarrow \quad \delta|_t = \gamma|_t \end{aligned} \tag{11}$$

with

S	$-h^2 - y^2 + 2cy$	[m^2]

Simultaneously, some small penetration of the weathering front will occur in that same interval, on top of the penetration that had already been achieved at time *t*. The erosion during Δt will however remove some of the weathered material that was present at time *t* and therefore the additional weathering penetration leads to a smaller depth than suggested on the basis of the weathering depth $D_w|_t$ alone. Depending on how much of the weathered material is removed by erosion (none, some or all), the maximum increase of the weathering depth at any height *z* is only partially obtained. With $D_{w,y}$ being the horizontal weathering depth, measured along the *y*-axis (Figure 3), the weathering depth is given by:

$$\begin{aligned} D_{w,y}|_{t+\Delta t} &= \frac{D_w|_t + e^{A+BD_w|_t}\Delta t}{\sin(\delta|_t)} - \Delta y_e \\ &\text{if } \frac{e^{A+BD_w|_t}\Delta t}{\sin(\delta|_t)} - \Delta y_e > 0 \\ D_{w,y}|_{t+\Delta t} &= D_{w,y}|_t = \frac{D_w|_t}{\sin(\delta|_t)} \\ &\text{if } \frac{e^{A+BD_w|_t}\Delta t}{\sin(\delta|_t)} - \Delta y_e = 0 \\ D_{w,y}|_{t+\Delta t} &= \max\left(0; \frac{D_w|_t + e^{A+BD_w|_t}\Delta t}{\sin(\delta|_t)} - \Delta y_e\right) \\ &\text{if } \frac{e^{A+BD_w|_t}\Delta t}{\sin(\delta|_t)} - \Delta y_e < 0 \end{aligned} \tag{12}$$

The first line in Equation (12) represents a case where penetration of weathering can exceed erosion, the second

In a similar way, the weathering penetration extending vertically downward from the (assumed) horizontal surface above the slope can be taken into account. Any weathering depth along the slope profile and the top surface above it predating excavation can also be incorporated by adapting the boundary condition of Equation (14) to reflect the pre-existing weathering profile.

In the above equations it is assumed that the coefficients *A* and *B* are not influenced by the presence of a scree cover, in other words that for the rock covered by scree and for the rock that is not yet covered, the same coefficients *A* and *B* can be used. Although it is generally accepted (Heimsath *et al.*, 1997; Martin, 2000) that the penetration rate of a weathering front decreases with increasing penetration depth with uneroded weathered material acting as a protective cover over the unweathered part of a rock mass, it is quite possible that a cover of loose slope waste such as scree, with a higher porosity than the *in situ* material it is covering, may retain more water after rainfall than the *in situ* rock and enhance the potential for chemical weathering. In rock types where chemical weathering processes are dominant, this would lead to higher weathering rates for scree-covered sections of the slope profile. If weathering penetration rates thus change because of the influence of a scree cover, this can be included in the iteration by defining A_c and B_c in Equation (12) for all $z < z_{int}$, and A_s and B_s for all $z \ge z_{int}$ ($A_c \ne A_s$ and $B_c \ne B_s$, with the indices $_c$ and $_s$ indicating 'covered by scree' and 'slope surface', respectively). For the results presented, *A* and *B* have, however, been kept constant for simplicity.

Field Investigations

The model derived in this paper has been calibrated for a small road cut near the village of Gavadà in the Tarragona province in Spain (Figure 4). This slope was studied for several years after its excavation in relatively fast-weathering shales. The

Figure 4. Gavada study slope, May 2004.

research done at this slope is described in detail by Huisman (2006).

The Gavadà case study slope was excavated during the reconstruction of a small road leading from the C-233 main road towards Gavadà. For the reconstruction works, which were executed in 1999, a number of road cuts had to be made. Since a considerable stretch of the road alignment runs through Keuper shales, this reconstruction provided the opportunity to monitor the rapid decay of these shales. The study slope consists of such shales, intercalated with thinly to very thinly bedded dolomitized limestones. Although it is ~50 m long, the slope is fairly small, with a maximum height of ~2 m.

The shales weather more rapidly, and erode more easily than the dolomites and therefore the rate of retreat of this slope is controlled by the shales. Their decay is predominantly determined by the presence of clays in combination with pronounced changes in water content at the surface induced by rain, sun and wind. Due to the resulting wetting and drying cycles, the shales swell and shrink repeatedly, and the associated volume changes will lead to weakening of the material by the repeated tensile and compressive stresses. These strains and the break-up of material bonds at the microscopic scale (Kühnel, 2002) lead to a slaking and loosening of material at the surface, which is then easily eroded mainly by gravitational processes as well as splash erosion and sheet wash in wet periods and deposited at the toe of the slope, a process defined as pelitoclastesis by Wetzel and Einsele (1991). Other processes such as hydrolysis may well occur simultaneously but the effects of these are not dominant. The main clay mineral present in the Keuper shales in the study slope is illite (21% by volume), but swelling capacity is determined mainly by the montmorillonite content of approximately 4% by volume. The swelling/shrinking behaviour is associated with considerable slaking. Laboratory tests on these shales show a second cycle slake durability shales of only 17% ('low durability', Dick and Shakoor, 1995).

Apart from the observations made in the study slope described in this paper, a number of other artificial slopes made in the same lithologies have been investigated, describing the weathering intensity as well as the weathering rate. In the context of this study weathering *intensity* refers to the degree of decomposition at one particular moment in time, whereas the weathering (intensity) *rate* refers to the amount of change in this weathering intensity per unit time. We have added the word 'intensity' to the weathering rate here, to distinguish it from the weathering penetration rate – which is a quantity for the rate of advance of a weathering penetration front.

Overall, there is a clear trend that the weathering intensity rates increase with an increasing amount of intercalated shales, and the highest weathering intensity rates are observed in slopes facing the sun and dominant wind during rainfall and are therefore exposed to the most pronounced wetting and drying cycles (Huisman *et al.*, 2006).

Model Calibration

For the combined erosion–weathering model, processes along the slope were simplified to down-wasting or denudation whatever actual form these may have (rolling, sliding, water erosion, mud flows, etc.) and to depth-dependent weathering which mobilizes material for erosion. Even so, this simple model demonstrates the complexities for practical observations on decay in slopes. The model exhibits three variables y, z and t, and six parameters R_s, a, b, c, A and B that need to be quantified. These parameters were calibrated for the Gavadà case study slope described above.

Since its excavation, significant erosion has taken place in this slope. A succession of cross-sections of the slope surface measured at the location of the traffic sign (Figure 4) is shown in Figure 5. At this location, the slope height is 2.05 m. As is apparent from these cross-sections, erosion debris accumulates

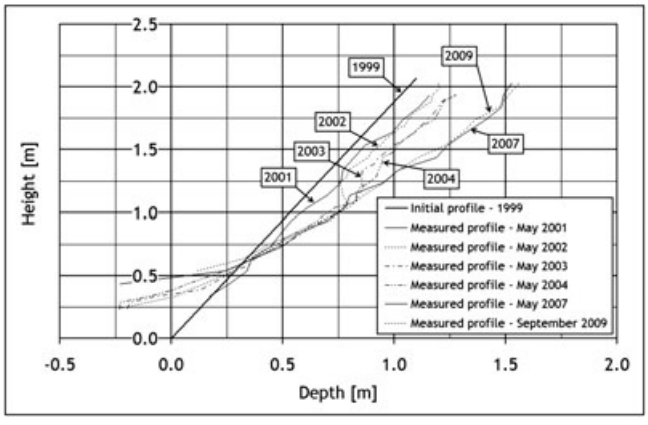

Figure 5. Cross-sections of the Gavada slope.

at the foot of the slope, whereas the top of the slope recedes.

The initial slope angle was 62°. The stable angle of the erosion debris was determined to be approximately 35° by measuring the stable angle of repose of a small pile of scree collected from the slope. Thus the parameters a and b of the erosion model are taken as cot(35) and cot(62), respectively. It is noted that a constant scree angle and therefore a constant value for a is valid for relatively small slope heights only, since the scree profile at the slope toe would have a concave profile for high slopes in which the fall energy of particles, which decreases as the slope development progresses, has a notable influence on the angle of repose.

A comparison of the eroded volume and the debris volume in each cross-section shows that a larger volume erodes than what is actually present as scree at the foot of the slope. The 'missing' debris is transported away from the slope by rainfall runoff; a ditch at the toe of the slope connects to a culvert and a small circular pond, where the eroded and transported material accumulates. On average, the volume of eroded rock is approximately twice the volume of the remaining scree, resulting in a negative value for c ($c = 1 -$ (volume of rock)/(volume of scree) $= -1$).

In Figure 6 the inclination of the apex through the upper section of the slope is plotted against time. For the first 5 years after excavation this angle γ decreased at an approximately linear rate of 1.2°/year. The latest measurement seems to indicate that this rate of retreat is decreasing. This would be in line with the data reported by Hutchinson (1998), which also suggested a decreasing rate of slope retreat. However, the time span covered by the observations in the study slope is too short to verify this, and for the present paper a linear rate of $R_s = 1.2°$/year has been assumed as an example. A non-linear decrease of γ can nevertheless easily be incorporated in the model (in fact any function would be allowed for $\gamma(t)$).

In order to confirm the uniform rotating retreat mechanism that is assumed for the Bakker–Le Heux model used in this paper, a detailed scan was made of a part of the slope in May 2004 with an Optech Ilris 3D laser scanner. This provided a high resolution point cloud with x, y and z-coordinates and reflection intensity for each of the reflection points (see Slob and Hack (2004) for a description of this LIDAR method). The resulting point cloud was compared with the initial planar slope surface. By calculating the retreat of the slope in a horizontal direction for each reflection point, a contour plot can be made showing the amount of erosion or accumulation. The results showed erosion contours with respect to the original excavated slope surface that are approximately parallel to the toe of the slope, with accumulation in the bottom section of the slope and an increasing amount of erosion towards the top, in accordance with the rotating retreat model (Huisman, 2006). Since the contours showed uniform amounts of erosion over the length of the slope, the development shown in the local cross-sections of Figure 5 is considered representative for the entire slope.

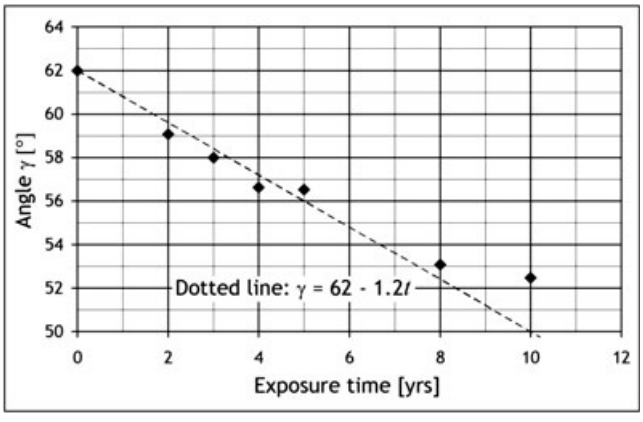

Figure 6. Development of gamma with time.

While the erosion parameters are relatively easy to obtain from a sequence of slope cross-sections, the parameters related to the weathering penetration are more difficult to quantify. In the study slope, small excavations were made at sufficient distance from the cross-section location so as not to influence future measurements, to estimate the penetration depth of the weathering front. In 2004, 5 years after excavation, it was found that the irregular pattern of disintegrated weak material covering the slope turned into a weak rock with clearly distinguishable discontinuity sets, with a block size of approximately 4 to 5 cm, within 10 to 12 cm from the slope surface and at a height of 1 m above the toe of the slope. This transition was taken as the depth of the weathering front. Since erosion occurs on the surface, it is not possible to directly compute the Heimsath A and B parameters of Equation (7) or W_s in the simplified Equation (9), which would otherwise simply be equal to $W_s = D_w / \ln(1 + t)$. Therefore the combined erosion-weathering model was run to find the best fitting value for these parameters. It was found that in combination with the linear slope retreat rate of $R_s = 1.2°$/year, values of $W_s = 0.1$ m/ln(year), $A = \ln(W_s) = -2.30$, and $B = -1/W_s = -10$ gave a good match for the weathering penetration depth estimated from the excavations. Due to the destructive nature of determining the weathering penetration depth by excavation this was not repeated in later years, and finding representative values for A and B remains a difficult aspect of the method presented in this paper.

Example of Modelling Results

Figures 7 and 8 show results of a numerical calculation based on the model described above, using the parameters calibrated for the Gavadà case study slope. The example calculations exclude weathering from the top surface for ease of interpretation. If this is included, the top parts of the slope will be affected by that too, and weathering depths calculated for the top of the slope will be larger than on the basis of weathering from the slope surface alone.

The model parameter values used for these graphs are given in Table I. Figure 7 shows the calculated slope profile at different exposure times, with the eroded rock core, a scree cover, and the weathering penetration front. The development of the modelled slope through the years as shown in Figure 7 indicates that (when assuming constant values for R_s, a and c) after some 20 years a situation will be reached in which the final convex shape of the rock core is reached, the whole slope is covered by scree, and erosion has come to an end. Before this occurs, the section of the eroded rock face that is not covered by scree extends linearly upward, creating a knick point at the intersection with the convex section underneath the scree cover, and the surface of the scree itself. This same knick point is reflected in the weathering penetration front; this is most pronounced in Figure 7(c). Note that for an exposure time of 5 years the cross-section of May 2004 has been included in the figure. The modelled and measured profiles are a close match but obviously this also results from the fact that the model parameters that describe the erosion process have been derived directly from the set of cross-sections.

Although cross-sections as in Figure 7 are visually appealing, a better insight into the fine balance between erosion and weathering is obtained in the graphs in Figure 8, which show the thickness of the weathered layer perpendicular to the slope

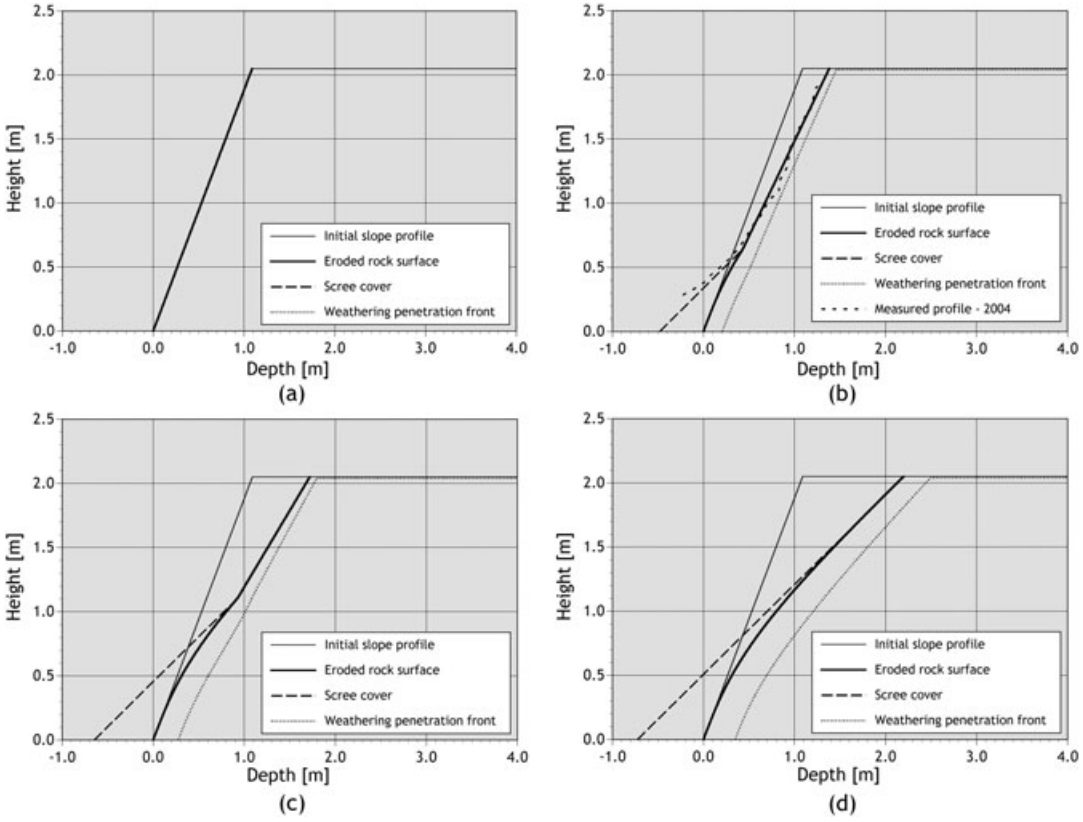

Figure 7. Examplesof modelling results for Gavadà slope, for different exposure times and corresponding years (excavation in 1999): (a) exposure time 0 years; (b) exposure time 5 years; (c) exposure time 10 years; (d) exposure time 20 years.

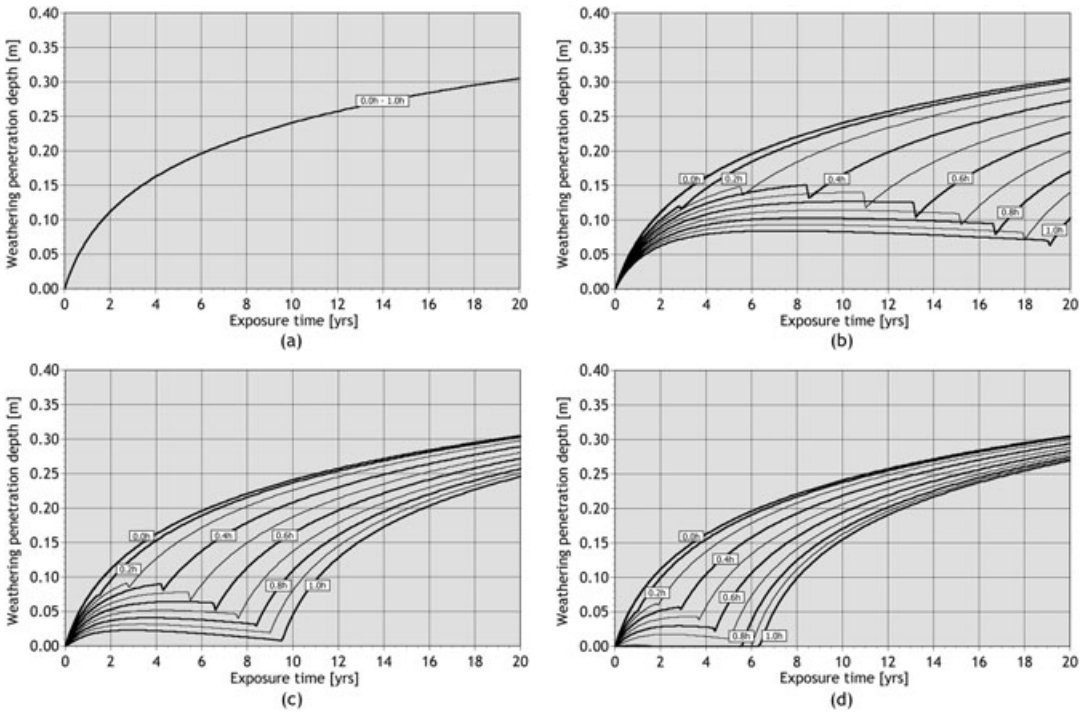

Figure 8. Example of modelling results weathering depths changing in time, for different rates of slope retreat: (a) 0° per year; (b) 1° per year; (c) 2° per year; (d) 3° per year.

surface as a function of (exposure) time. Figure 8(a) shows the result for the case where the rate of slope retreat is set at 0°/year, so zero erosion. A single curve is found representing points at all heights throughout the slope profile. Since the simplified Heimsath model was assumed to derive A and B from field observations, with $A = \ln(W_s)$ and $B = -1/W_s$, this curve is given by Equation (9).

Figure 8(b)–(d) presents cases where erosion rates in terms of slope angle decrease are larger than zero. Points at different heights in the slope profile now show different curves; lines are given for points at 0.0*h, 0.1*h, 0.2*h, ..., 1.0*h (with h the slope height). At the foot of the slope (height 0.0*h), no erosion occurs and the same curve as in Figure 8(a) is obtained; this is the limiting situation, visible in all graphs of Figure 8(b)–(d).

Table I. Model parameters used for results shown in Figure 7

Parameter	Symbol	Value	Unit
Stable angle of scree	α	35	[°]
Initial slope angle	β	62	[°]
Slope height	h	2.05	[m]
1–(volume of rock)/(volume of scree)	c	−1.0	[−]
Rate of slope retreat	R_s	1.2	[°/yr]
Weathering penetration parameter	A_s	−2.30	[−]
Weathering penetration parameter	B_s	−10	[1/m]
Weathering penetration parameter	A_c	−2.30	[−]
Weathering penetration parameter	B_c	−10	[1/m]

The curves representing the development of a weathered layer at the other points do however show clear differences.

In the graphs of Figure 8(b) and (c), with erosion rates of 1°/year and 2°/year, a weathering layer develops at the start of the decay processes at all heights in the slope profile; this can be recognized as an increase in the weathering thickness (rising curves) although not as fast as in the limiting case for the curve representing height 0.0*h. These initially rising curves represent decay situations where some erosion occurs, but an imbalance favouring weathering exists. The curves for points higher in the slope profile tend to become horizontal after some time; this signifies equilibrium between erosion and weathering penetration, resulting in a constant thickness of the weathered zone. Some curves even develop a negative slope signifying a decrease in the thickness of the weathered zone, and therefore an imbalance favouring erosion. This may even extend to the case where the weathered layer disappears altogether with D_w becoming zero (a situation almost reached in Figure 8(c) for 1.0*h). All curves finally trend upward again after a sudden knick point. This knick point occurs at the time at which the scree extends to the height that is represented by each curve, resulting in erosion coming to an end at that particular height. The small sharp step, which is also visible in most curves at this knick point, results from the step-wise change of the slope angle at this specific point in time. This causes the weathering depth perpendicular to the slope to have a discontinuous first-order derivative. In the limiting case of $t \rightarrow \infty$ all curves tend to become equal to the curve for 0.0*h, implying that the whole slope is then covered by scree and erosion has ended, and the simplified Heimsath relation of Equation (9) applies.

Figure 8(d) shows the same basic decay situations existing at various times and locations; however, with the relatively high erosion rate of 3°/year, the curves for the upper section of the slope profile show a zero thickness of the weathered zone until the scree has built up to that particular height. These horizontal curves at $D_w = 0$ represent a decay situation in which erosion outpaces weathering, and no weathering mantle can establish itself because any weathered material is continuously eroded (a weathering-limited situation). With a further increase in erosion rates, the knick points at which the scree wedge passes the height represented by each curve will shift to the left, towards shorter exposure times. In the limiting case for $R_s \rightarrow \infty$ the final slope profile is reached after an infinitely short time, and all curves will fall on the same line again, given by Equation (9).

Points at different heights in the slope profile will generally be in different decay situations at the same time, and the decay situation at a specific location may change in time. The most homogeneous slope development will occur with either very small (relative to weathering penetration rates) erosion rates, or with very large erosion rates (again relative to weathering penetration rates). With intermediate combinations of erosion and weathering penetration rates, the upper slope will tend to show imbalance favouring erosion whereas the lower slope will show imbalance favouring weathering.

Discussion and Conclusions

The model derived in this paper combines the Bakker–Le Heux erosion model (with rotating slope retreat mechanism) with a weathering penetration model in which the weathering penetration rate decreases with increasing thickness of the weathering cover. The resulting set of equations has been solved numerically by time-stepping, and gives both the slope profile and the weathering front as a function of time. The simplicity of the derived conceptual model may well be preferable over more sophisticated process-based models for predictions based on scarce observations on actual slopes or for back-analysis of existing slopes. Although in this paper the model parameters have been assumed to remain constant in time for simplicity, the modelling approach allows for time-variable parameters, most notably for the erosion parameters R_s, a and c.

An interesting discussion point is the general observation in the study area that the rotational Bakker–Le Heux model for slope evolution is the better fit for the observations. In this model the down wasting is represented by the erosion of triangular slices that are thick at the top and thin at the toe. At first sight this may seem to be in conflict with the modelling results presented in Figures 7 and 8, which show that in all cases the weathering penetration depth is greater at the toe than at the top of the slope section which is not covered by scree material. It must be noted that if the slope profile development is transport-limited, with an imbalance of decay processes favouring weathering and the rate of erosion and transport of weathered material being the limiting factor, removal of sediment from the slope surface will not be related to the depth of the weathering front (at least if the degree of weathering on the slope surface does not vary over the slope height). As long as this situation remains, weathered material accumulates, and transport processes act at their full capacity (Kirkby, 1971). As shown in Huisman (2006), the slope profile development in the study area and the case study slope is indeed almost uniquely transport-limited.

The better fit of the rotational slope development model must therefore be explained from the following factors: the possibility of a higher weathering intensity at the top of the slope, due to the existence of an old weathering mantle parallel to the original (natural) slope profile before excavation, increasing the soil erodibility near the top; weathering from the top of the slope, which is not incorporated in the results shown in Figures 7 and 8 (but can easily be included in the model), and the specific transport processes. Although no detailed observations have been made regarding the latter, it is believed that soil creep and sheet wash are the dominant transport processes in the study slope.

Depending on erosion and weathering penetration rates, various possible decay situations are shown to occur at a given point in time for different locations along the slope profile, just as different situations occur for a given location along the slope profile for different exposure times. This is demonstrated for a linear decrease of the slope angle with time; the qualitative results are independent of the precise nature of this particular trend.

The most homogeneous slope development will occur with either very small (relative to weathering penetration rates) or zero erosion rates, or with very large erosion rates (again relative to weathering penetration rates). Intermediate combinations of erosion and weathering penetration rates will cause different behaviour in the upper and lower parts of the slope. It has to be noted that the lower part of a slope may be covered by scree after some time, which will probably affect the weathering penetration rate in that part. Different penetration

rates for these parts of the slope can easily be incorporated in the model but this does not affect the general shape of the curves as presented in Figure 8.

The greatest difficulty in determining realistic values for the parameters of this model lies with the determination of the weathering depth and weathering penetration parameters *A* and *B*. For the study presented in this paper these were estimated based on a few shallow and destructive excavations. Future research should investigate the possibilities of non-destructive techniques to monitor the weathering depth (e.g. ground radar based methods).

In engineering practice, models such as the one presented in this paper can help to predict the development of a slope profile excavated in a weak rock in time. With the addition of strength parameters to the weathering profile, the presented model may be extended to serve as the basis for the prediction of the stability of slopes in weak rock as a function of time as well. Perhaps of even greater value is that the model results clearly show just how intricate the balance between erosion and weathering in a slope can become, and that this balance will change and shift in time and vary for different locations in the slope. This implies that rock mass classifications and slope stability assessments carried out in the field may not only be a snapshot at a particular time, but also a snapshot of a particular location in a slope. With this understanding, engineers in the field shall carefully assess whether even with a single lithology, a slope is actually homogeneous enough in terms of weathering and erosion to warrant a classification as a single unit, or that the slope needs to be split up into various levels with a similar development.

References

Ahnert F. 1976. Brief description of a comprehensive three-dimensional process-response model of landform development. *Zeitschrift für Geomorphologie, Supplement* **25**: 29–49.

Anderson RS, Humphrey NF. 1989. Interaction of weathering and transport processes in the evolution of arid landscapes. In *Quantitative Dynamic Stratigraphy*, Cross TA (ed). Prentice-Hall: Englewood Cliffs, NJ; 349–361.

Bakker JP, Le Heux JWN. 1946. Projective-geometric treatment of O. Lehmann's theory of the transformation of steep mountain slopes. *Proceedings Koninklijke Nederlandse Akademie van Wetenschappen (KNAW)* **49**(5): 533–547.

Bakker JP, Le Heux JWN. 1952. A remarkable new geomorphological law. The law of the denudation slope with recti-linear cross-profile I-III. *Proceedings Koninklijke Nederlandse Akademie van Wetenschappen (KNAW)* **55**(4): 399–410 and 554–571.

Brazier RE, Beven KJ, Freer J, Rowan JS. 2000. Equifinality and uncertainty in physically based soil erosion models – application of the GLUE methodology to WEPP for sites in the UK and USA. *Earth Surface Processes and Landforms* **25**: 825–845.

Carson MA. 1969. Models of hillslope development under mass failure. *Geographical Analysis* **1**: 76–100.

Dick JC, Shakoor A. 1995. Characterizing durability of mudrocks for slope stability purposes. In *Clay and Shale Slope Instability - Reviews in Engineering Geology Volume X*, Haneberg WC, Anderson SA (eds). The Geological Society of America: Boulder, CO; 121–130.

Heimsath AM, Dietrich WE, Nishiizumi K, Finkel RC. 1997. The soil production function and landscape equilibrium. *Nature* **388**: 358–361.

Hencher SR, McNicholl DP. 1995. Engineering in weathered rock. *The Quarterly Journal of Engineering Geology* **28**: 253–266.

Huisman M. 2006. Assessment of rock mass decay in artificial slopes. PhD thesis, ITC, Enschede.

Huisman M, Hack HRGK, Nieuwenhuis JD. 2006. Predicting rock mass decay in engineering lifetimes: the influence of slope aspect and climate. *Environmental and Engineering Geoscience* **12**(1): 39–51.

Hutchinson JN. 1998. A small-scale field check on the Fisher-Lehmann and Bakker-Le Heux cliff degradation models. *Earth Surface Processes and Landforms* **23**: 913–926.

Kirkby MJ. 1971. Hillslope process-response models based on the continuity equation. In *Slopes Form and Process*, Brunsden D (ed). Institute of British Geographers, London, UK: Special Publication no. 3; 15–30.

Kühnel RA. 2002. Driving forces of rock degradation. In *Proceedings Protection and Conservation of the Cultural Heritage of the Mediterranean Cities*, Sevilla, Spain, Galán and Zezza (eds). A.A. Balkema: Rotterdam; 11–17.

Martin Y. 2000. Modelling hillslope evolution: linear and nonlinear transport relations. *Geomorphology* **34**: 1–21.

Nieuwenhuis JD. 1991. *The Lifetime of a Landslide; Investigations in the French Alps*. Balkema: Rotterdam.

Slob S, Hack HRGK. 2004. 3D terrestrial laser scanning as a new field measurement and monitoring technique. In *Engineering Geology for Infrastructure Planning in Europe. A European Perspective*, Hack HRGK, Azzam R, Charlier R (eds). Springer Verlag: Berlin; 179–190.

Tucker GE, Slingerland RL. 1994. Erosional dynamics, flexural isostasy, and long-lived escarpments: a numerical modeling study. *Journal of Geophysical Research* **99**: 12229–12243.

Wetzel A, Einsele G. 1991. On the physical weathering of various mudrocks. *Bulletin of the International Association of Engineering Geology* **44**: 89–99.